Analytica Chimica Acta 1260 (2023) 341206

Contents lists available at ScienceDirect

Analytica Chimica Acta

journal homepage: www.elsevier.com/locate/aca

Investigation of the adsorption/desorption mechanism of perfluoroalkyl substances on HLB-WAX extraction phases for microextraction

Aghogho A. Olomukoro [a,b], Charlotte DeRosa [b,d], Emanuela Gionfriddo [a,b,c,*]

[a] Department of Chemistry and Biochemistry, The University of Toledo, Toledo, OH, 43606, USA
[b] Dr. Nina McClelland Laboratories for Water Chemistry and Environmental Analysis, The University of Toledo, Toledo, OH, 43606, USA
[c] School of Green Chemistry and Engineering, The University of Toledo, Toledo, OH, 43606, USA
[d] College of Pharmacy and Pharmaceutical Sciences, The University of Toledo, Toledo, OH, 43606, USA

HIGHLIGHTS

- PFAS adsorption and desorption mechanisms on HLB-WAX were investigated.
- 15 PFAS with an alkyl chain from C_4 to C_{14} and different chemical functionalities were targeted.
- SPME fiber and thin film geometries were evaluated to provide optimal extraction efficiency.
- Screening of PFAS in seawater, melted snow and human plasma was performed via SPME-LC-MS/MS.

GRAPHICAL ABSTRACT

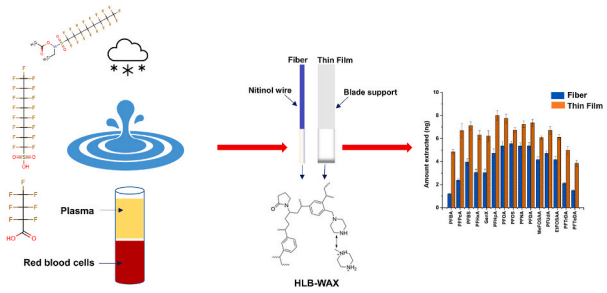

ARTICLE INFO

Handling Editor: Xiu-Ping Yan

Keywords:
Ion-exchange sorbents
Solid phase microextraction
Perfluoroalkyl substances

ABSTRACT

The *C*–F alkyl structural backbone of per- and polyfluoroalkyl substances makes this class of molecules resistant to heat and degradation, leading to their high persistence and mobility in the environment and bioaccumulation in the tissues of living organisms. In this study, 15 PFAS with an alkyl chain length from C_4 to C_{14}, currently monitored by the U.S. Environmental Protection Agency (EPA), were preconcentrated by solid-phase microextraction (SPME) and analyzed by liquid chromatography-tandem mass spectrometry. The adsorption and desorption mechanisms of PFAS onto ion-exchange extraction phases was evaluated to understand the extraction process of PFAS from various environmental matrices under different conditions. This was achieved using two SPME geometries, namely fibers and thin films. The use of thin films resulted in a twofold improvement in extraction efficiency compared to fibers, especially for the short-chain PFAS. Methanol:water (80:20, v/v) was chosen as the optimized desorption solution, with ammonium formate added to minimize carryover. Extraction time profiles for both SPME geometries showed faster equilibration with thin films (30 min) compared to fibers (90–120 min). The linear dynamic range obtained with this method using fibers and thin films ranged from 10 to 5000 ng L^{-1} and 2.5–5000 ng L^{-1}, respectively, with acceptable accuracy (70–130%) and precision (<15%). LOD ranged within 2.5–10 ng L^{-1} for fibers and 0.01–0.25 ng L^{-1} for thin films. Investigating the factors affecting PFAS recovery in complex samples enabled the quantitative assessment of PFAS contamination in various environmental water samples such as seawater, melted snow and biospecimens like human plasma. A 96-SPME holder was used for validation, which is compatible with sampling in 96-well plates and ensures high throughput

* Corresponding author. Department of Chemistry and Biochemistry, The University of Toledo, Toledo, OH, 43606, USA.
E-mail address: emanuela.gionfriddo@utoledo.edu (E. Gionfriddo).

https://doi.org/10.1016/j.aca.2023.341206
Received 23 December 2022; Received in revised form 24 March 2023; Accepted 9 April 2023
Available online 10 April 2023

in the analysis of real samples. The total concentration of PFAS detected in seawater and snow was 51.3 ng L^{-1} and 16.4 ng L^{-1}, respectively.

Abbreviations

C18	Octadecyl silica
EDS	Energy dispersive x-ray spectroscopy detector
EtFOSAA	*N*-ethyl perfluorooctanesulfonamidoacetic acid
EPA	Environmental protection agency
ESI	Electrospray ionization
GenX	Hexafluoropropylene oxide dimer acid
HESI	Heated electrospray ionization
HLB	Hydrophilic-lipophilic balance
HLB-WAX/PAN	Hydrophilic-lipophilic balance/polyacrylonitrile
LOD	Limit of detection
LOQ	Limit of quantification
MeFOSAA	*N*-methyl perfluorooctanesulfonamidoacetic acid
MRM	Multiple reaction monitoring
PAN	Polyacrylonitrile
PBS	Phosphate-buffered saline
PFAS	Per and poly fluoroalkyl substances
PFBA	Perfluoro butanoic acid
PFBS	Perfluorobutanesulfonic acid
PFDA	Perfluorodecanoic acid
PFPeA	Perfluoropentanoic acid
PFHxA	Perfluorohexanoic acid
PFOA	Perfluorooctanoic acid
PFOS	Perfluorooctanesulfonic acid
PFHpA	Perfluoroheptanoic acid
PFNA	Perfluorononanoic acid
PFTrDA	Perfluorotridecanoic acid
PFTeDA	Perfluorotetradecanoic acid
PFUdA	Perfluoroundecanoic acid
SEM	Scanning electron microscope
SPME	Solid phase microextraction
WAX	Weak anion exchange

1. Introduction

The widespread use of perfluoro- and polyfluoroalkyl substances, commonly known as PFAS in the manufacturing industry has led to increasing environmental contamination. Thus it is becoming critical for environmental monitoring and public health protection to accurately detect PFAS in water, biota, and complex environmental samples [1,2]. PFAS structure consists of a polar functional group, usually a carboxylic or sulfonic acid, connected to either a fully (per-) or partially (poly-) fluorinated alkyl chain [3,4]. The fluorinated alkyl backbone of PFAS is hydrophobic and lipophobic (i.e., it is not attracted to water or nonpolar organic substances). This is because the *C*–F bond is symmetrically arranged in the alkyl chain, which causes PFAS's low overall polarizability. This low polarizability also means a weak van der Waals interaction. Therefore, fluorinated compounds are immiscible with both water and organic solvents, forming a three-phase system [5,6]. These orthogonal properties that characterize PFAS, allow this class of molecules to easily disperse at interfaces of heterogeneous systems, such as air and water [7]. In addition to this unique chemistry, the strength and stability of *C*–F bonds contribute to the high persistence and mobility of PFAS in the environment, as well as bioaccumulation in animals, plants and human tissues [8,9].

Most PFAS are ionized in aqueous environments and thus can be readily transported through aqueous systems, and oceans are considered an important sink for these pollutants. PFAS are released directly into rivers through the discharge of industrial effluents, landfills, and sewage, and in due course, enter the marine environment [10]. Long-range transport of volatile and semi-volatile PFAS precursors can lead to degradation into ionic PFAS (such as carboxylic and sulfonic acids), which are considered potential PFAS sources in remote areas [11]. Precipitations are among effective pathways to remove PFAS from the atmosphere, as PFAS have been detected in snow [12], rainwater [13,14] and stormwater [15,16]. However, with the varying composition of these water samples, matrix effects during chemical analysis may pose a challenge due to their salinity and/or the presence of dissolved organic matter that may co-elute with the PFAS of interest [17,18]. Filtration of these samples could be an option; however, this may result in loss of analytes or cross-contamination of samples. Furthermore, because of the high risk posed by the release of PFAS into the environment and their ability to bioaccumulate in living organisms, it is important to study PFAS not only in aqueous media but also in biological samples, such as blood or plasma, to establish a link between environmental contamination and human exposure. Commonly used techniques for the determination of PFAS in complex samples include filtration [19], solvent extraction [20], and solid phase extraction (SPE) [21]. These methods have limitations, such as a long sample preparation time, high solvent and sample consumption, and the risk of cross-contamination of complex samples due to multiple sample pretreatment steps [22]. Therefore, techniques to improve selectivity and efficient enrichment while minimizing matrix effects are critical for high-precision monitoring of PFAS in the environment and biological samples.

Microextraction methods provide a valid alternative to the above techniques to improve preconcentration and reduce the use of organic solvents, resulting in a more sensitive and environmentally friendly extraction strategy. SPME is characterized by its versatility and applicability to a wide range of samples because of its ability to perform both headspace and direct sampling of complex systems through the use of biocompatible extraction phases [23–25]. Several SPME geometries are available and have been explored in various applications such as air, water, soil, and biological sampling [24], with fiber geometry being the most commonly used SPME configuration. However, if method sensitivity is an issue, alternative geometries such as thin films can be used to increase extraction efficiency. In addition, thin film SPME allows for a large surface area to volume ratio of the extraction phase, which improves extraction kinetics [26,27]. The use of biocompatible extraction phases also allows extraction from complex samples such as biofluids and tissues by minimizing biofouling of the extraction devices and co-extraction of sample interferences [28]. Polyacrylonitrile (PAN) is the most commonly used biocompatible polymer for SPME-LC applications. PAN is hydrophilic and has good chemical stability and anti-biofouling properties that prevent the adhesion of macromolecules that cause fouling. This is due to a hydration layer, which is formed by hydrogen bonds between the functional groups on the surface of the device and the water molecules in the sample [29]. These properties make PAN optimal for SPME use in biological fluids, tissues, and food analysis. Its good chemical stability allows desorption in organic solvents and prevents swelling of the extraction phase.

Commonly used sorbents for PFAS are C_{18} [30], HLB [31,32], WAX

[33,34] and mixed mode phases coupled to a weak anion exchange (WAX) moiety [35,36]. In our previous study [37], HLB-WAX/PAN provided best recoveries and balanced extraction coverage for 4 representative PFAS (C_4, C_6 and 2 C_8). In this study, we expanded the number and type of PFAS investigated to include PFAS with alkyl chain ranging from C_4 to C_{14}, and with carboxylic, sulfonic and sulfonamidoacetic acid functionalities. Moreover, strategies to ensure PFAS quantitative desorption and reduce carryover on the HLB-WAX/PAN sorbent were also investigated. In our previous work [37], adding ammonium hydroxide into the desorption solution reduced the carryover on the HLB-WAX extraction phase to < 5%. However, it is still unclear whether the desorption mechanism is primarily due to the effect of pH on the WAX moieties or to an anion exchange interaction of the anionic PFAS and hydroxide ion on the extraction phase. Therefore, in this study the performance of HLB-WAX/PAN SPME devices for preconcentration of 15 PFAS were investigated, in order to (i) determine the mechanisms controlling the desorption of PFAS from the extraction phase and extraction of PFAS from the sample matrix, which is especially critical in the analysis of seawater and melted snow due to the presence of dissolved ions and organics in the sample that can affect selectivity, (ii) evaluate matrix effects in seawater, melted snow, and human plasma, (iii) develop a high-throughput method using 96-well plates for complex matrices, and (iv) assess how the extraction efficiency of PFAS changes in a biological matrix such as human plasma due to binding to native plasma components.

2. Materials and methods

2.1. Chemicals and supplies

All standards PFBA, PFePA, PFBS, PFHxA, PFHpA, GenX, PFOA, PFOS, PFDA, PFNA, CPFUdA, MeFOSAA, EtFOSAA, PFTrDA and PFTeDA were purchased from AccuStandard (New Haven, CT, USA). ^{13}C labeled internal standards ($^{13}C_8$ -PFOA, $^{13}C_8$ -PFOS, $^{13}C_3$ –GenX and $^{13}C_2$ – PFUdA) were obtained from Wellington Laboratories (Ontario, Canada). Other properties of these analytes are listed in Table S1. Ultrapure water from a Nanopure Infinity System (Barnstead, Thermofisher Scientific) was used as mobile phase A. LC-MS grade methanol and isopropanol were purchased from Birch Biotech (Morgantown, PA), ammonium formate, ammonium acetate and ammonium hydroxide from Fisher Scientific (Hampton, NH), ammonium fluoride from Acros Organics, and ammonium chloride from Sigma Aldrich (St. Louis, MO, USA). A seasalt mixture used to produce simulated seawater samples was purchased from Lake Products Company LLC, MO, USA. The composition of the sea salt mixture is listed in Table S2. Phosphate-buffered saline (PBS) and human plasma preserved with sodium citrate were purchased from Sigma Aldrich and Innovative Research (MI, USA), respectively. *N*,*N*-dimethylformamide and polyacrilonitrile (PAN) were purchased from Acros Organics and Sigma Aldrich respectively. HLB-WAX particles were purchased from Waters Corporation (Milford, MA). C18/PAN and HLB/PAN fibers were kindly provided by Millipore Sigma (Bellefonte, PA, USA) and HLB-WAX/PAN fibers and thin films were prepared according to the procedures described in our previous work [37]. The length of the extraction phases was 1 cm and their thickness is as follows: the C18/PAN thickness 42 μm, HLB/PAN 37 μm, HLB-WAX/PAN fiber and thin film were 35 μm and 190 μm, respectively. The nitinol wire and blades were purchased from Component Supply Company (Sparta, TN) and Yarder Manufacturing Co. (Toledo, OH), respectively.

2.2. Sample collection and storage

All water samples were collected in high-density polyethylene bottles as recommended by US EPA [38]. Snow was collected after accumulation in Februray 2022 at the University of Toledo campus and allowed to melt in a refrigerator before being frozen at −20 °C. Real seawater samples were collected at North Myrtle Beach in South Carolina and stored in the refrigerator until analysis. The human plasma was stored in the freezer at −20 °C until analysis.

2.3. Fiber and thin film preparation

The fibers and thin films (deposited on a metal blade) were prepared by dip coating using a dip coater (Ni-Lo X2 Dip Coater, Ottawa, Canada). Briefly, 5 g of polyacrilonitrile and 72.5 mL of dimethylformamide were placed in a beaker and heated to 90 °C for 1 h and then cooled. A slurry was then prepared by mixing the HLB-WAX particles with the above solution and stirring overnight before coating. The nitinol wires were cleaned in a sonicator in methanol for 30 min, while the blades were etched with 220 grit sandpaper and cleaned in methanol: isopropyl alcohol (50:50, v/v) for 15 min. Both the fibers and blades were coated by dipping them in the slurry to a length of 1 cm and cured in an oven at 125 °C for 1 min. On average, a total of 6 layers of extraction phase were deposited on fibers and 4 layers on the metal blades to ensure a homogeneous coating. The inter-batch reproducibility for both fibers and thin films is shown in Fig. S1.

2.4. SPME procedure

A 96-well plate robot (PAS technology Deutschland GmbH, Germany) (Fig. S2) was used for extraction and desorption of the water samples. For plasma samples, an agitator was used for extraction from 700 μL plastic vials and the 96-well plate for desorption. Extraction was performed for 20 min in a 2 mL plastic plate with 96 wells. Sample volume was 500 μL for plasma and 1 mL for water. For the desorption process, a 350 μL 96-well plate (MicroSolv, Leland NC) with a glass insert was used and desorption was performed for 20 min. 150 μL desorption solution of methanol:water (80:20, v:v) with 0.5% (w:w) ammonium formate was used for the SPME fiber procedure. For SPME thin film, desorption was performed in 250 μL of methanol:water (80:20, v:v) desorption solution with 2% (w:w) ammonium formate. Both extraction and desorption were performed at a speed of 1000 rpm. After extraction from the plasma samples, a short rinsing step was performed in ultrapure water to remove any loosely adhering particles on the fibers and thin films before immersion in the desorption solution.

2.5. Working standard preparation

All working standards and stock standards were prepared and stored in methanol at 4 °C except PFOA individual stock standard solution, that was stored at – 20 °C. PFTeDA and PFTrDA stock standards, were stored in 50:50 methanol:water according to manufacturer's recommendation.

2.6. Instrumentation and data processing

A QSight LX50®binary UHPLC pump, autosampler, and column compartment (PerkinElmer Inc., Waltham, MA, USA) with a PerkinElmer Brownlee SPP C_{18} column (50 mm × 3 mm, 2.7 μm) was used for chromatographic separation, with the column compartment kept at 30 °C. A Restek PFAS delay column C_{18}, (50 × 2.1 mm, 3 μm) (Restek Corporation, Bellefonte, PA) was used to trap and delay PFAS in the system to ensure accurate and reliable quantification. The total run time was 10 min with an injection volume of 10 μL (partial loop injection, total loop size 20 μL). Ultrapure water (A) and methanol (B), both containing 2.5 mM ammonium acetate, were used as the mobile phase for the gradient. At a flow rate of 0.5 mL/min, the mobile phase gradient started at 5% B from 0 to 1.0 min and then increased to 45% at 1.5 min. It was then maintained at 98% B from 7 to 8.0 min and finally decreased to 5% B from 8.1 to 10 min. The QSight 220 ® (PerkinElmer Inc. Waltham, MA, USA), a triple quadrupole mass spectrometer was used for detection and quantification of analytes in negative heated electrospray ionization (HESI) mode. Multiple Reaction Monitoring (MRM) was used

to monitor all target analytes and internal standards. Nitrogen gas for the ESI source, the laminar flow ion guide, and collision cell was generated by a Parker/Balston nitrogen generator system (Parker Hannifin Corporation, Lancaster, NY, USA). The optimized MS conditions were: ESI voltage −2300 V, drying gas and nebulizer gas 100 and 300, respectively, source and HSID temperature 300 °C and 200 °C, respectively. Table S1 shows the analytes' MS/MS transitions, including the internal standards.

A JEOL JSM -7500 F scanning electron microscope (SEM) (JEOL USA, Inc., Peabody, MA) with a BRUKER XFlash 5010 series energy dispersive x-ray spectroscopy detector (EDS) (Billerica, MA) was used for surface morphology and thickness of SPME fiber and thin film. SEM images of the fibers and thin films can be found in Fig. S3.

Data acquisition and processing were performed using Simplicity 3Q®software (version August 1, 2006.12348) (PerkinElmer Inc., Waltham, MA, USA). Origin 9.0 (OriginLab Corporation, Northampton, MA, USA) was used for additional data processing. A mixture of standard solutions with concentrations ranging from 0.05 to 50 μg L^{-1} was used to calibrate the instrument and calculate the mass of PFAS extracted by the SPME fibers and thin films during method optimization.

2.7. Matrix effect and method validation

Matrix effects were studied for snow, seawater and human plasma based on the procedure proposed by Matuszewski et al. [39]. Extractions from blank samples and desorption in a methanol:water (80:20, v/v) solution were performed. After desorption, a mixture of PFAS standards was added to the desorption solution prior to instrumental analysis. Three concentrations of 25, 50, and 500 ng L^{-1} were analyzed for matrix effects. Similarly, ultrapure water and PBS were used as control samples for water and plasma, respectively. In addition to the control samples, the PFAS mixture was added to a pure desorption solution and analyzed. The absolute matrix effects were calculated using Equation (2.1).

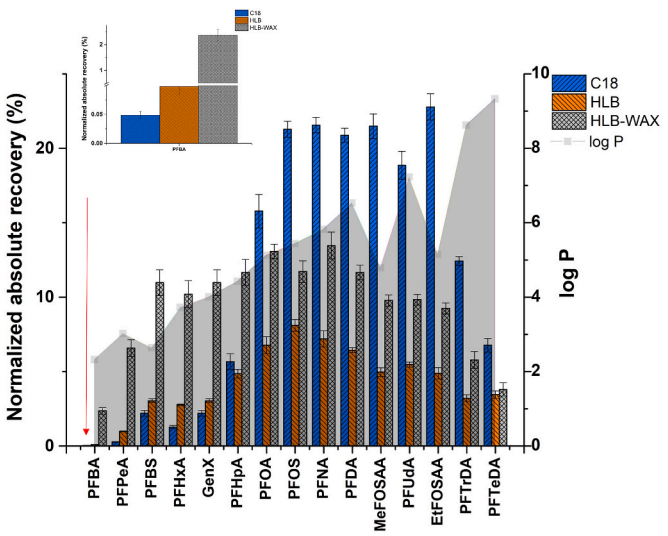

Fig. 1. Comparison of the absolute recovery normalized by extraction phase volume $\left(\frac{ng\ extracted}{ng\ spiked} * \text{volume of extraction phase}\right) * 100$ with different sorbents. Extraction and desorption time was at 90 min with agitation speed at 1000 rpm. Desorption solution was methanol:water (80:20, v/v).

other acids such as acetic acid, propionic acid, and n-butyric acid can enhance response in the negative mode, but this largely depends on the concentration and compounds of interest, as studied by Wu et al. [40]. This phenomenon can be attributed to the droplet surface (i.e., the accumulation of anions on the droplet surface leading to a change in local pH) and the relatively higher gas phase affinity of these acids compared to formic acid [41,42]. In addition, the use of ammonium formate and ammonium acetate was also compared to determine the optimum mobile phase composition (Fig. S5). Ammonium acetate

$$ME\% = \frac{post\ extraction\ spiked\ desorption\ solution}{post\ extraction\ spiked\ desorption\ solution\ control\ matrix\ or\ clean\ desorption\ solution}\ x\ 100 \qquad \text{Equation 2.1}$$

SPME calibration was performed by extraction from ultrapure water spiked with PFAS at concentrations of 0.25, 5, 15, 25, 50, 100, 250, 500, 1000, and 5000 ng L^{-1} for thin films and 10, 15, 25, 50, 100, 250, 500, 1000, and 5000 ng L^{-1} for fibers, with internal standards spiked at 150 ng L^{-1}. Extractions were performed in triplicate for each concentration. For instrumental analysis, extracts were injected in triplicate, giving a total of nine replicates for each concentration level. Linearity, linear dynamic range, accuracy, precision, limit of quantitation (LOQ) (evaluated as the lowest concentration in the calibration curve with accuracy between 70 and 130% and precision <20%), and limit of detection (LOD) (lowest concentration that can be accurately detected with a S/N ≥ 3) of the method were evaluated.

3. Results and discussion

3.1. Chromatographic conditions

Various mobile phase additives were added to ensure maximum sensitivity, especially for the more hydrophobic PFAS. Fig. S4 shows that the addition of 0.1% formic acid decreases the sensitivity of all analytes. Since PFAS are ionized in negative ESI mode, acidic conditions generally decrease negative ESI mode response and lower pH does not favor the formation of deprotonated acids [40]. However, it should be noted that favored the response of the most hydrophobic compounds (C_8–C_{14}), whereas ammonium formate enhanced that of PFBA and PFPeA, the two most polar compounds: the responses of other compounds were unchanged. Therefore, ammonium acetate was chosen as the optimal additive for the mobile phase.

3.2. SPME conditions

3.2.1. SPME extraction phase evaluation

The extraction efficiency of 15 PFAS was investigated with three different biocompatible sorbents, namely C18/PAN, HLB/PAN and HLB-WAX/PAN, compared at an extraction time of 90 min (Fig. 1). This evaluation was necessary to understand the interaction of the 15 PFAS, having different chemical structure, and functionality with the chemistry of the extraction phases. 90 min was chosen as the extraction time to bring the conditions as close to equilibrium as possible and to ensure maximum sensitivity for all sorbents [43]. It was observed that C_{18}/PAN extracted the longer-chain PFAS (C_8 - C_{14}) more efficiently than the shorter-chain compounds (C_4 - C_7) due to the strong hydrophobic interaction favoring the distribution of the longer-chain PFAS onto the extraction phase. This is due to the C–F bonds being symmetrically arranged in the PFAS alkyl chain, resulting in an overall nonpolar chain with low polarizability, so that the PFAS exhibit only weak van der Waals interactions [6]. In general, the hydrophobicity increases as the

carbon chain length increases, as shown by the number of carbons and log P values in Table S3. However, the use of C_{18}/PAN resulted in extraction discrimination, as the shorter chain PFAS compounds with log P values between 2.31 and 4.41, were poorly extracted. Absolute recoveries for these analytes with C_{18} ranged from 0.05 to 2.2%. HLB, on the other hand, provided balanced coverage of all analytes and improved extraction of shorter chain compounds compared to C_{18} (absolute recoveries of 0.10–3.0%). Balanced extraction coverage is a critical factor in multi-residues analysis because it avoids discrimination in the extraction of analytes with different chain lengths and chemical functional groups. Our results show that HLB-WAX/PAN not only provided balanced coverage of the 15 PFAS tested (C_4 - C_{14}), but also improved the extraction efficiency of all analytes compared to HLB and showed a twofold increase in the recovery of short-chain PFAS compared to C_{18}. These findings are in line with our previous study that only evaluated 2 C_8, 1 C_4 and C_6 PFAS and can be explained as a result of anion exchange between the negatively charged PFAS compounds and the WAX moieties, which are cationic between pH 1 and 5, whereas between pH 6 and 8 only one WAX moiety is cationic and the other is neutral [37]. Similarly, other studies have shown that using WAX SPE cartridges improves the extraction efficiency of anionic PFAS compared to HLB [44]. Therefore, HLB-WAX/PAN was chosen as the optimized extraction phase to efficiently extract the wide range of PFAS targeted in our study. It is worth mentioning that, if the more hydrophobic PFAS (i.e., those having a longer C $\geq$ 7 alkyl chain) are the primary targets for an analytical method, C_{18} can be alternatively used for improved extraction efficiency.

3.2.2. Fiber SPME and thin film SPME comparison

Since PFAS are present in the environment at trace and ultra-trace concentrations, improving the sensitivity, the kinetics of mass transfer between the sample and the extraction phase, and the overall throughput of the analysis is critical to achieving adequate sensitivity for environmental monitoring and human exposure assessment. However, reaching the desired sensitivity, especially with respect to the limits of quantification imposed by regulatory agencies, can be challenging due to the limited volume and chemistry of the extraction phase used [45]. Therefore, to improve extraction efficiency, two SPME geometries -fiber and thin film in blade format-were investigated. In addition, by using thin films, higher throughput can be achieved when analyzing water samples in 96-well plate format.

The solution to improve extraction performance was to increase the volume of the extraction phase, as explained in Supplementary Information Equation 3.1. This equation directly relates the amount of analytes extracted at equilibrium to the volume of the extraction phase. Increasing the volume of the extraction phase leads to an increase in extraction efficiency. However, increasing the volume of the extraction phase when using a fiber geometry leads to slower extraction kinetics, since the thickness of the extraction phase increases as a result [26,46]. Therefore, the equilibrium time may be longer compared to other geometries such as thin film. Hence, HLB-WAX/PAN was immobilized on a metal blade support, which provides a higher surface area-to -volume ratio and increases the extraction efficiency, as shown in Fig. 2A. The high surface area-to-volume ratio can enhance the sampling rate reducing the time necessary to reach equilibrium according to Equation 3.2 (Supplementary Information) [26].

Furthermore, fiber constant, a parameter useful in interpreting extraction efficiencies of different extraction phases, was calculated for both geometries. Fiber constant is defined as $f_c = K_{es}V_e$ for liquid coatings and as $f_c = K_{es}S_a$ for solid coatings. Where K_{es} is the distribution coefficient of the analyte (between the extraction phase and sample), V_e volume of extraction phase and S_a is the active surface of the fiber coating. However, the calculation of K_{es} for solid coatings requires the determination of solid extraction phase surface concentration S_e which can be expressed as the ratio of the amount extracted to the active surface of the solid coating, but the knowledge of the S_a value can be challenging to obtain. However, the fiber constant can also be calculated as shown in Equation (3.3) [47,48]:

$$f_c = \frac{n_e V_s}{V_s C_s - n_e} \qquad \text{Equation 3 .3}$$

As demonstrated in Fig. 2B, the fiber constants of PFAS gradually increases with an increase in hydrophobicity and then decreased for the later eluting analytes PFTrDA and PFTeDA. The lower fiber constant of PFTrDA and PFTeDA, the bulkier PFAS compounds targeted in this study, could be attributed to steric hindrance playing a role in their low extraction efficiency, making these molecules unable to properly interact with the WAX moieties for ion exchange.

Moreover, it was observed that the balanced extraction coverage by the HLB-WAX/PAN was more pronounced when using the thin film. The larger volume of the extraction phase in the thin film also resulted in improved extraction recovery of all analytes. This is important because PFAS compounds are found in the environment at parts per trillion concentrations and due to their ability to bind to biomolecules and organic matter, improved sensitivity is required to quantify them.

3.2.3. Optimization of extraction conditions

Different extraction conditions were evaluated and optimized for each SPME geometry. The extraction time profile was studied for both fiber and thin film. Fig. 3A and B shows extraction time profiles for five representative PFAS and Fig. S6 for all remaining analytes. The results show that equilibrium was reached after 30 min for all analytes when using the thin film, while equilibrium was reached after 90/120 min using the fiber, depending on the analyte. According to Equation 3.2 (Supplementary Information), this can be explained by the fact that the larger surface area to volume ratio not only ensures higher sensitivity,

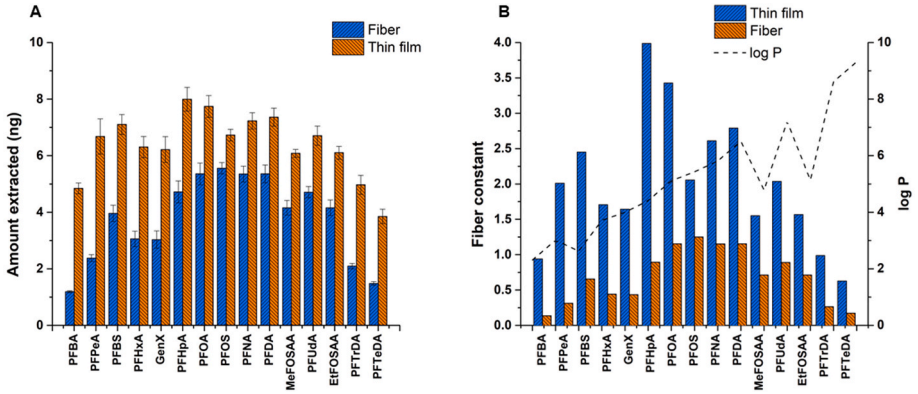

Fig. 2. A) Extraction performance of devices obtained at 90 min of extraction and desorption times with agitation speed at 1000 rpm. Desorption solution was methanol:water (80:20, v/v), B) Fiber constant calculated for both fiber and thin film.

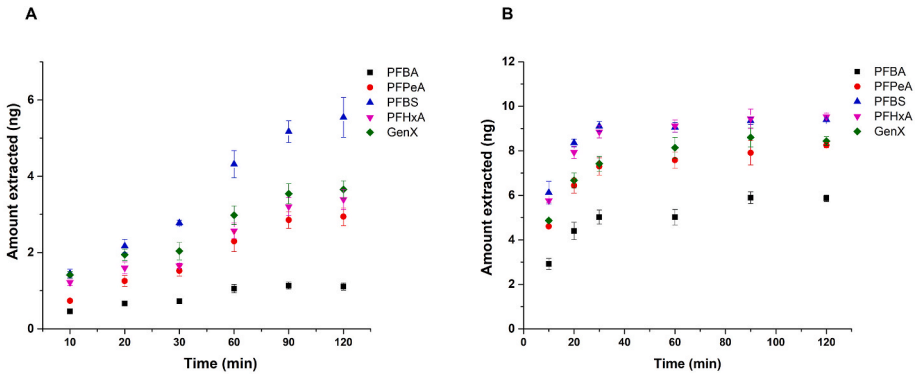

Fig. 3. Extraction time profile for PFBA, PFPeA, PFBS, PFHxA and GenX at 10, 20, 30, 60, 90 and 120 min using A) fibers and B) thin films.

but also improves the kinetics of extraction and thus shortens the time to reach equilibrium [26,46,49]. 20 min allowed both geometries to extract a sufficient amount of PFAS while maintaining high throughput. Therefore, 20 min was chosen as the optimized extraction time for both geometries (fiber and thin film). However, when sensitivity is a challenge, longer extraction times can be used.

3.2.4. Sample volume optimization

In SPME, the amount of analyte extracted is directly proportional to the sample volume (Equation 3.1 - Supplementary Information) [23]. In the laboratory, the sample volume is limited (usually 1–20 mL) due to the size of commercial vials and their compatibility with automated systems. For field applications, the sample volume can be large and its effect on the amount of analyte recovered becomes insignificant when $V_s \gg K_{es}V_e$ because Equation 3.1 reduces to Equation 3.4.

$$n_e = K_{es}V_eC_s \qquad \text{Equation 3.4}$$

In this study, the effect of sample volume on analyte recovery was investigated at two different extraction times (20 and 90 min) for both fibers and thin films (Figs. S7 and S8) to ensure the best compromise between adequate sensitivity, extraction time and high throughput of this method. It was found that the increment in the amount of analytes extracted at 20 min at increasing sample volumes was not as significant as at 90 min. This is because, at equilibrium conditions, analytes have enough time to reach the extraction phase from the bulk of the solution and diffuse through the boundary layer, moreover the maximum amount of analytes is extracted at the different sample volumes, which is not the case at pre-equilibrium conditions. The effect of sample volume on the extracted amount becomes negligible, especially for analytes with small fiber constants such as PFBA as seen in Fig. S6 [23,50]. In contrast, extraction efficiency of analytes with high fiber constants (PFOA, PFOS, PFDA, PFNA, etc.) is strongly dependent on sample volume.

1 mL was chosen as the optimal sample volume because it provided desirable sensitivity. In addition, a sample volume of 1 mL is compatible with the use of 96-well plates, which are available for high-throughput analyses.

3.2.5. Ionic strength

The effect of ionic strength on sorption of PFAS onto the HLB-WAX phase was investigated by simulating salinity of natural water bodies. Simulated seawater was prepared from a commercially available sea salt mixture containing ten different salts at varying compositions as found in natural seawater. The salt mixture includes NaCl, $MgCl_2{\cdot}6H_2O$, Na_2SO_4, $CaCl_2$, KCl, $NaHCO_3$, $SrCl_2{\cdot}6H_2O$, and NaF in the order of their occurrence in natural seawater. Table S2 shows the composition of the salt mixture and the conductivity measurements for solutions prepared at different salinity levels. Simulated seawater was prepared according to the manufacturer's description and samples at varying ionic strength were prepared from the undiluted (100%) seawater by dilution with ultrapure water. This experiment aimed to understand how levels typical of different types of environmental waters can affect the interaction of PFAS on the extraction phase, thus affecting recoveries compared to extraction from ultrapure water.

The tested samples were labeled as follows: 0% (contains only ultrapure water), 5% (contains 5% seawater and 95% ultrapure water), 75% (contains 75% seawater and 25% ultrapure water), and 100% (seawater only), etc. Fig. S9A shows the ionic strength evaluation using HLB-WAX/PAN. The amount of extracted analytes for the short-chain PFAS (PFBA (C_4), PFPeA (C_5), PFBS (C_4), PFHxA (C_6), GenX (C_6) and PFHpA (C_7)) showed no significant change as the salt concentration increased, except for the initial increase in recovery from ultrapure water to 5% seawater. However, for the later eluting compounds, i.e., PFOA (C_8), PFOS (C_8), PFNA (C_9), PFDA (C_{10}), the amount extracted decreased with increasing ionic strength starting from solution at 10% seawater. For MeFOSAA (C_{11}), PFUdA (C_{11}), EtFOSAA (C_{12}), PFTrDA (C_{13}) and PFTeDA (C_{14}), a decrease in the recovery was significant even at lower values of ionic strength (e.g. 5% seawater solution). These trends could be explained taking into account two phenomena: (1) the addition of salt may affect water solubility for the most hydrophobic PFAS, increasing their propensity for the adsorption on solid surfaces of the vial and thus reducing the partition coefficient of the extraction phase [51], (2) considering that the electrostatic interactions that take place between the WAX moiety and the PFAS are dependent on the relative distance among charges, shorter chain PFAS can interact strongly with the extraction phase while bulkier PFAS have a weaker interaction and can be easily displaced on the extraction phase by negative ions added in the solution. Moreover, to further corroborate this hypothesis, an HLB/PAN extraction phase containing no ion exchange components was also tested at various ionic strengths (Fig. S9B). For the analytes with carbon length C_4–C_9, the extraction efficiency increased with increasing salt concentration, showing the typical effect of salting out [52]. Interesting trends were observed for PFOA and PFOS both having C_8 perfluorinated chain but different head groups, a carboxylate and a sulfonate respectively. The recovery of PFOA increased with increasing ionic strength, while for PFOS, increasing recovery were observed up to 20% seawater solution with decreasing recovery obtained at higher ionic strength. The difference in trends may be related to the different polar surfaces of PFOA (37 $Å^2$) and PFOS (63 $Å^2$). The larger polar surface area of PFOS may enhance the interaction with silanol groups on the wall of the glass vials, leading to the adsorption of PFOS on the vials when water solubility is affected by ionic strength. This similarity becomes more apparent with increasing carbon length (i.e., C_{10} - C_{14}).

3.3. Desorption conditions

3.3.1. Desorption solution

After optimization of the extraction conditions, fine-tuning of the

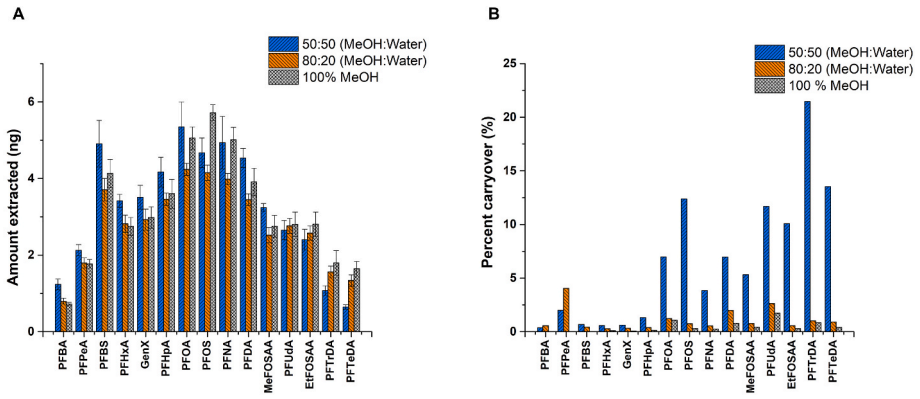

Fig. 4. Desorption solution optimization A) First desorption B) Percent carryover. 10 μg L^{-1} spiked in 1 mL of sample solution at 1000 rpm. Desorption was carried out in 320 μL 100% methanol, methanol:water (80:20, v:v), methanol:water (50:50, v:v).

desorption solution is required. To achieve maximum sensitivity and minimize carryover in the extraction phase, desorption solutions of 100% methanol, methanol:water (50:50, v:v), and methanol:water (80:20, v:v) were evaluated (Fig. 4A).

Methanol:water (50:50, v/v) as desorption solution resulted in a higher amount of desorbed analytes for most compounds, except for PFTrDA and PFTeDA. To verify presence of carryover, a second desorption was performed. The percent carryover with methanol:water (50:50, v/v) was above the acceptable limits (>15%) for the longer-chain C_8–C_{14} PFAS (Fig. 4B). The possible reason for this high carryover is that methanol:water (50:50, v/v) has a weak solvent strength and cannot remove a sufficient amount of PFAS from the extraction phase. This hypothesis is supported by the fact that, liquid chromatographic separation on a C_{18} stationary phase reveals that the mobile phase composition to elute PFTrDA and PFTeDA consists of 15% water and 85% methanol. 100% methanol and methanol:water (80:20, v/v) resulted in similar desorption efficiency and low percent carryover. However, the use of 100% methanol causes peak distortion for early eluting PFAS as a consequence of injection solvent mismatch [53]. Therefore, methanol:water (80:20, v:v) was used as the optimized desorption solution.

3.3.2. *Desorption solution additives*

In our previous work [37], adjusting the pH of the desorption solution to 10 using ammonium hydroxide drastically reduced the carryover when using HLB-WAX extraction phase. We hypothesized that the driving desorption mechanism involved the amino groups on the piperazine moieties on the HLB-WAX sorbent to become neutral at pH 10, facilitating quantitative desorption. Therefore, 0.05% ammonium hydroxide was added to all desorption solutions.

However, it was uncertain whether the negligible percent carryover after addition of ammonium hydroxide in the desorption solution was only due to the effect of pH on the charges of the WAX moieties or to an anion displacement effect between the negatively charged PFAS and the OH^- ions present in solution. Therefore, the mechanism driving the desorption of PFAS from HLB-WAX was further investigated by adding ammonium salts (ammonium formate, ammonium hydroxide, ammonium fluoride and ammonium chloride) with different counter ions to the desorption solution. Different concentrations of each salt added to the desorption solution were studied, namely 0.05, 0.3, 0.5 and 2% (w/v %). The obtained % carryover for these desorption solutions was compared to values obtained in pure solvent (0%- no salt addition). While the amount of analytes desorbed was not significantly affected by the addition of salt (Fig. S10), likely due to variation of carryover within the experimental error, it was observed that the addition of salt was necessary to further reduce the percent carryover (Fig. S11). From this experiment, we hypothesize that the anions of the ammonium salts (Cl^-, OH^-, COO^-, and F^-) compete with the negatively charged PFAS for the anion exchange interaction on the extraction phase and this phenomenon drives the desorption mechanism. The pH of the desorption solution containing ammonium salts (as specified in the caption for Fig. S11) were different and only ammonium hydroxide provided pH values able to neutralize the –NH groups on the WAX sorbent. Although ammonium hydroxide provided the lowest percent carryover, ammonium formate was used as the optimized additive to the desorption solution because it provided the best signal stability for a long series of consecutive LC-MS runs (n > 20).

3.3.3. *Desorption volume optimization*

It was observed that when working with thin films, the % carryover was higher than for fibers due to the greater amount of extraction phase on the device. Therefore, the desorption volume was optimized with different ammonium salts, such as ammonium hydroxide and ammonium formate at different volumes (320 μL and 500 μL) (Fig. S12A). Desorption volumes ≤320 μL resulted in better preconcentration but higher carryover. Therefore, a second and third consecutive desorption for the fiber and thin film was performed after the desorption process (Figs. S12B and S12C) to verify residual carryover. 150 and 250 μL were selected as optimal volumes for the fibers (Fig. S13) and thin films, respectively. 250 μL was chosen for the thin films because the use of 150 μL was not sufficient to completely cover the extraction phase which could lead to less reproducible results. In addition, a time profile for desorption was established for both geometries and 20 min was selected as the optimal time with low carryover (Fig. S14).

3.4. *Method validation and environmental samples analysis*

The optimized extraction and desorption conditions (extraction and desorption time, desorption solution, desorption volume, solution and additives and sample volume) were further used to create SPME calibration curves by spiking ultrapure water at concentrations ranging from 10 to 5000 ng L^{-1} for fibers and 2.5–5000 ng L^{-1} for thin films. LOQ values ranged from 10 to 100 ng L^{-1} and 2.5–50 ng L^{-1} for fibers and thin films, respectively. LOD for SPME fiber was 2.5 ng L^{-1} for all analytes except PFTrDA, which was 5 ng L^{-1} and PFTeDA 10 ng L^{-1}. 0.01 ng L^{-1} was the LOD achieved with thin film with the exception of PFTeDA which was 0.25 ng L^{-1}. The results showed that the use of a thin film achieved a wider linear dynamic range and a lower LOQ and LOD, especially for the hydrophilic and hydrophobic compounds. This indicates that the use of thin film is crucial for the detection of PFAS concentrations in the sub-parts per trillion range. The linearity, LOQ and LOD values obtained for all analytes are presented in Table 1. Tables S4 and S5 show the accuracy and precision values obtained for all analytes with fiber and thin film within acceptable limits, as stated by US EPA, between 70 and 130% [38]. Selected chromatograms obtained for analytes injected at the LODs values for both geometries are shown in

Table 1
R^2, linearity and weighting for all analytes obtained using SPME thin film and SPME fiber.

SPME Thin film					SPME Fiber				
Analyte	R^2	LDR (ng L^{-1})	LOD (ng L^{-1})	Weighting	Analyte	R^2	LDR (ng L^{-1})	LOD (ng L^{-1})	Weighting
PFBA	0.997	2.5–5000	0.01	1/x	PFBA	0.997	15–5000	2.5	1/x
PFPeA	0.998	2.5–5000	0.01	1/x	PFPeA	0.995	10–5000	2.5	1/x
PFBS	0.993	2.5–5000	0.01	1/x	PFBS	0.996	10–5000	2.5	1/x
PFHxA	0.998	2.5–5000	0.01	1/x	PFHxA	0.995	10–5000	2.5	1/x
GenX	0.998	2.5–5000	0.01	1/x	GenX	0.994	10–5000	2.5	1/x
PFHpA	0.999	2.5–5000	0.01	1/x	PFHpA	0.999	10–5000	2.5	1/x
PFOA	0.999	2.5–5000	0.01	1/x	PFOA	0.998	10–5000	2.5	1/x
PFNA	0.999	2.5–5000	0.01	1/x	PFNA	0.999	10–5000	2.5	1/x
PFOS	0.997	2.5–5000	0.01	1/x	PFOS	0.998	15–5000	2.5	1/x
PFDA	0.997	5–5000	0.01	1/x	PFDA	0.996	15–5000	2.5	1/x
MeFOSAA	0.996	15–5000	0.01	1/x	MeFOSAA	0.994	25–5000	2.5	1/x
PFUdA	0.997	15–5000	0.01	1/x	PFUdA	0.996	15–5000	2.5	1/x
EtFOSAA	0.997	5–5000	0.01	No weighting	EtFOSAA	0.996	25–5000	2.5	1/x
PFTrDA	0.993	25–5000	0.01	1/x	PFTrDA	0.995	50–5000	5	1/x
PFTeDA	0.982	50–5000	0.25	1/x	PFTeDA	0.980	100–5000	10	1/x

Fig. S15.

The calibration curves obtained were further used to quantify PFAS content in environmental waters. Analysis of seawater and snow samples was performed by spiking internal standards at 150 ng L^{-1}. Table S6 and Fig. S16 demonstrated that some of the targeted PFAS were detected in the real samples while PFPeA, GenX, PFTeDA and PFOS were not detected in seawater or snow water. PFAS detected in both seawater and snow water are PFBA, PFHxA, PFOA, PFNA, PFDA, PFUdA, PFTrDA, EtFOSAA and MeFOSAA.

Matrix effects evaluation was performed in snow and seawater to validate the accuracy of our results. The evaluation could only be performed for analytes that were not present in any of the water samples. Minimal ion enhancement was observed for PFPeA at 25 ng L^{-1} for seawater and snow, as demonstrated in Table S7. As our results in section 3.2.2 predicted, seawater presented higher matrix effects due to the effects of ionic strength on the extraction efficiency. In light of this, a matrix-matched calibration in seawater or a standard addition method are recommended for accurate quantification of PFAS in seawater samples.

3.5. Extraction of PFAS from human plasma

Strategies for biomonitoring of PFAS in human biofluids are critical for assessing environmental exposure. Considering the biocompatibility of PAN-based extraction phases used in this work a proof of concept to demonstrate the applicability of our method for PFAS analysis in human plasma was performed. The amount of PFAS extracted from PBS and plasma samples was compared to demonstrate the sensitivity of the developed method for human plasma, which is a complex sample that includes binding agents (Fig. S17). As the figure illustrates, the amount extracted from plasma was significantly lower than that of PBS. This indicates the presence of PFAS binding to the plasma components compared to PBS with no binding matrix. Matrix effects assessment was performed with human plasma and minimum to no matrix effect was observed using both fibers and thin film devices, expect for PFBA and PFPeA (Table S8). Furthermore, extraction from pooled human plasma was performed revealing that PFBA and PFPeA were detected, this is the reason why the matrix effect for these two compounds are above acceptable values. Fig. S18 shows the overlay of the fiber blank and plasma blank, indicating the presence of these compounds in the plasma.

4. Conclusion

This work presents a thorough investigation of extraction and desorption mechanisms on ion exchange extraction phases for 15 PFAS. The desorption mechanism of PFAS from the ion-exchange extraction phase HLB-WAX/PAN was determined using ammonium salts with different counterions, and it was deduced that the anion-exchange interaction is the dominant interaction in the desorption of PFAS rather than the effect of pH on the charges of the WAX moiety.

Two SPME geometries - fiber and thin film - were evaluated to improve not only the sensitivity of extraction but also the kinetics of mass transfer, leading to high throughput. The use of thin film proved necessary to increase sensitivity, especially for monitoring contaminants at low part per trillion levels with LOD values as low as 0.01 ng L^{-1}. Good linearity, accuracy, and precision were obtained with this method. LOQ ranged from 10 to 100 ng L^{-1} for fiber geometry and 2.5–50 ng L^{-1} for thin film. The LOQ values obtained were below the latest (March 2023) USEPA proposed limit (4 ng L^{-1}) for PFOA and PFOS in drinking water. 11 of the 15 PFAS studied were present in seawater and snow, with the exception of GenX, PFPeA, PFOS, and PFTeDA. The amount of PFAS extracted from PBS and human plasma shows that the free concentration of PFAS in plasma is lower due to binding to plasma components. The negligible matrix effects obtained in human plasma indicate the suitability of HLB WAX-PAN SPME devices for PFAS environmental monitoring and human exposure assessment. PFBA and PFPeA were present in the human plasma sample analyzed, however, it remains uncertain whether the presence of these PFAS was due to post-sampling contamination, as a third party collected these samples for commercial purposes.

CRediT authorship contribution statement

Aghogho A. Olomukoro: Methodology, Validation, Formal analysis, Investigation, Visualization, Data curation, Writing – original draft. **Charlotte DeRosa:** Methodology. **Emanuela Gionfriddo:** Conceptualization, Supervision, Project administration, Funding acquisition, Writing – review & editing.

Declaration of competing interest

The authors declare that they have no known competing financial interests or personal relationships that could have appeared to influence the work reported in this paper.

Data availability

Data will be made available on request.

Acknowledgements

This work was funded by the National Oceanic and Atmospheric Administration (NOAA), award # NA18OAR4170100 (Ohio Sea Grant College Program R/PS-056 subaward # 60074859) and the National

Science Foundation (CAREER # 2144591). The authors are thankful to PerkinElmer Inc., for enabling the use of the QSight®200, in particular to Dr. Erasmus Cudjoe, Dr. Qiao Hui and Jesse Cornejo for the continuous support and technical assistance. The authors also acknowledge Supelco-Millipore Sigma for providing the HLB-PAN fibers used in this work.

Appendix A. Supplementary data

Supplementary data to this article can be found online at https://doi.org/10.1016/j.aca.2023.341206.

References

[1] R. Loos, S. Tavazzi, G. Mariani, G. Suurkuusk, B. Paracchini, G. Umlauf, Analysis of emerging organic contaminants in water, fish and suspended particulate matter (SPM) in the Joint Danube Survey using solid-phase extraction followed by UHPLC-MS-MS and GC–MS analysis, Sci. Total Environ. (2017) 607–608, https://doi.org/10.1016/j.scitotenv.2017.07.039, 1201–1212.

[2] R.C. Buck, J. Franklin, U. Berger, J.M. Conder, I.T. Cousins, P. De Voogt, A. A. Jensen, K. Kannan, S.A. Mabury, S.P.J. van Leeuwen, Perfluoroalkyl and polyfluoroalkyl substances in the environment: terminology, classification, and origins, Integr. Environ. Assess. Manag. 7 (2011) 513–541, https://doi.org/10.1002/ieam.258.

[3] J.F. Ayala-Cabrera, A. Contreras-Llin, E. Moyano, F.J. Santos, A novel methodology for the determination of neutral perfluoroalkyl and polyfluoroalkyl substances in water by gas chromatography-atmospheric pressure photoionisation-high resolution mass spectrometry, Anal. Chim. Acta 1100 (2020) 97–106, https://doi.org/10.1016/j.aca.2019.12.004.

[4] V. Boiteux, X. Dauchy, C. Bach, A. Colin, J. Hemard, V. Sagres, C. Rosin, J. F. Munoz, Concentrations and patterns of perfluoroalkyl and polyfluoroalkyl substances in a river and three drinking water treatment plants near and far from a major production source, Sci. Total Environ. 583 (2017) 393–400, https://doi.org/10.1016/j.scitotenv.2017.01.079.

[5] K.J. Harris, K.J. Harris, Occurrence of Per- and Polyfluoroalkyl Substances in Cosmetics and Personal Care Products by Affairs in Partial Fulfillment of the Requirements for the Degree of, 2022.

[6] H.J. Lehmler, Synthesis of environmentally relevant fluorinated surfactants - a review, Chemosphere 58 (2005) 1471–1496, https://doi.org/10.1016/j.chemosphere.2004.11.078.

[7] J.A.K. Silva, W.A. Martin, J.L. Johnson, J.E. McCray, Evaluating air-water and NAPL-water interfacial adsorption and retention of Perfluorocarboxylic acids within the Vadose zone, J. Contam. Hydrol. 223 (2019), 103472, https://doi.org/10.1016/j.jconhyd.2019.03.004.

[8] F. Pérez, M. Nadal, A. Navarro-Ortega, F. Fàbrega, J.L. Domingo, D. Barceló, M. Farré, Accumulation of perfluoroalkyl substances in human tissues, Environ. Int. 59 (2013) 354–362, https://doi.org/10.1016/j.envint.2013.06.004.

[9] A.O. De Silva, J.M. Armitage, T.A. Bruton, C. Dassuncao, H. Bernays, X.C. Hu, PFAS exposure pathways for humans and wildlife: a synthesis of current knowledge and key gaps in understanding, Environ. Toxicol. Chem. 40 (2021) 631–657, https://doi.org/10.1002/etc.4935.

[10] Q. Wang, M.M.P. Tsui, Y. Ruan, H. Lin, Z. Zhao, J.P.H. Ku, H. Sun, P.K.S. Lam, Occurrence and distribution of per- and polyfluoroalkyl substances (PFASs) in the seawater and sediment of the South China sea coastal region, Chemosphere 231 (2019) 468–477, https://doi.org/10.1016/j.chemosphere.2019.05.162.

[11] K.Y. Kwok, E. Yamazaki, N. Yamashita, S. Taniyasu, M.B. Murphy, Y. Horii, G. Petrick, R. Kallerborn, K. Kannan, K. Murano, P.K.S. Lam, Transport of Perfluoroalkyl substances (PFAS) from an arctic glacier to downstream locations: implications for sources, Sci. Total Environ. 447 (2013) 46–55, https://doi.org/10.1016/j.scitotenv.2012.10.091.

[12] G. Shan, X. Chen, L. Zhu, Occurrence, fluxes and sources of perfluoroalkyl substances with isomer analysis in the snow of northern China, J. Hazard Mater. 299 (2015) 639–646, https://doi.org/10.1016/j.jhazmat.2015.07.074.

[13] S. Taniyasu, K. Kannan, L.W.Y. Yeung, K.Y. Kwok, P.K.S. Lam, N. Yamashita, Analysis of trifluoroacetic acid and other short-chain perfluorinated acids (C2-C4) in precipitation by liquid chromatography-tandem mass spectrometry: Comparison to patterns of long-chain perfluorinated acids (C5-C18), Anal. Chim. Acta 619 (2008) 221–230, https://doi.org/10.1016/j.aca.2008.04.064.

[14] P. Suwannakot, F. Lisi, E. Ahmed, K. Liang, R. Babarao, J.J. Gooding, W.A. Donald, Metal–organic framework-enhanced solid-phase microextraction mass spectrometry for the direct and rapid detection of perfluorooctanoic acid in environmental water samples, Anal. Chem. 92 (2020) 6900–6908, https://doi.org/10.1021/acs.analchem.9b05524.

[15] S.T. Wolf, W.K. Reagen, Method and validation for the analysis of perfluorinated compounds in water by pre-sampling isotope dilution-direct injection-LC/MS/MS, Anal. Methods 5 (2013) 2444–2454, https://doi.org/10.1039/c3ay26347a.

[16] C.A. Moody, Wai Chi Kwan, J.W. Martin, D.C.G. Muir, S.A. Mabury, Determination of perfluorinated surfactants in surface water samples by two independent analytical techniques: liquid chromatography/tandem mass spectrometry and 19F NMR, Anal. Chem. 73 (2001) 2200–2206, https://doi.org/10.1021/ac0100648.

[17] E. Rianawati, R. Balasubramanian, Optimization and validation of solid phase micro-extraction (SPME) method for analysis of polycyclic aromatic hydrocarbons in rainwater and stormwater, Phys. Chem. Earth 34 (2009) 857–865, https://doi.org/10.1016/j.pce.2009.07.003.

[18] E. Boyaci, K. Goryński, C.R. Viteri, J. Pawliszyn, A study of thin film solid phase microextraction methods for analysis of fluorinated benzoic acids in seawater, J. Chromatogr. A 1436 (2016) 51–58, https://doi.org/10.1016/j.chroma.2016.01.071.

[19] T. Jiawei, Z. Yizhen, S. Jiajun, S. Xuelu, S. Chao, Z. Chunhui, Occurrence and characteristics of perfluoroalkyl substances (PFASs) in electroplating industrial wastewater, Water Sci. Technol. 79 (2019) 731–740, https://doi.org/10.2166/wst.2019.092.

[20] B.F. Da Silva, A. Ahmadireskety, J.J. Aristizabal-Henao, J.A. Bowden, A rapid and simple method to quantify per- and polyfluoroalkyl substances (PFAS) in plasma and serum using 96-well plates, MethodsX 7 (2020), 101111, https://doi.org/10.1016/j.mex.2020.101111.

[21] K. Palmer, J.T. Bangma, J.L. Reiner, R.K. Bonde, J.E. Korte, A.S.P. Boggs, J. A. Bowden, Per- and polyfluoroalkyl substances (PFAS) in plasma of the West Indian manatee (Trichechus manatus), Mar. Pollut. Bull. 140 (2019) 610–615, https://doi.org/10.1016/j.marpolbul.2019.02.010.

[22] N. Luque, A. Ballesteros-Gómez, S. van Leeuwen, S. Rubio, A simple and rapid extraction method for sensitive determination of perfluoroalkyl substances in blood serum suitable for exposure evaluation, J. Chromatogr. A 1235 (2012) 84–91, https://doi.org/10.1016/j.chroma.2012.02.055.

[23] J. Pawliszyn, Handbook of Solid Phase Microextraction, Chemical Industry Press, Beijing, 2009.

[24] A. Naccarato, A. Tagarelli, Recent applications and newly developed strategies of solid-phase microextraction in contaminant analysis: through the environment to humans, Separations 6 (2019) 2–43, https://doi.org/10.3390/separations6040054.

[25] N.H. Godage, A.A. Olomukoro, R.V. Emmons, E. Gionfriddo, In vivo analytical techniques facilitated by contemporary materials, TrAC, Trends Anal. Chem. 142 (2021), 116290, https://doi.org/10.1016/j.trac.2021.116290.

[26] R.V. Emmons, R. Tajali, E. Gionfriddo, Development, optimization and applications of thin film solid phase microextraction (TF-SPME) devices for thermal desorption: a comprehensive review, Separations 6 (2019), https://doi.org/10.3390/separations6030039.

[27] G.A. Gómez-Ríos, N.R. Garcés, M. Tascon, Smart materials in solid phase microextraction (SPME), Handb.Smart.Mater.Anal.Chem. (2019) 581–620, https://doi.org/10.1002/9781119422587.ch18.

[28] E. Gionfriddo, Biocompatible microextraction devices for simple and green analysis of complex systems, LCGC North Am. 38 (2020). Number s6.

[29] E. Gionfriddo, Biocompatible microextraction devices for simple and green analysis of complex systems, LC-GC Eur. 38 (2020) 25–29.

[30] C.P. Higgins, J.A. Field, C.S. Criddle, R.G. Luthy, Quantitative determination of perfluorochemicals in sediments and domestic sludge, Environ. Sci. Technol. 39 (2005) 3946–3956, https://doi.org/10.1021/es048245p.

[31] Y. Jeong, K.M. Da Silva, E. Iturrospe, Y. Fuiji, T. Boogaerts, A.L.N. van Nuijs, J. Koelmel, A. Covaci, Occurrence and contamination profile of legacy and emerging per- and polyfluoroalkyl substances (PFAS) in Belgian wastewater using target, suspect and non-target screening approaches, J. Hazard Mater. 437 (2022), 129378, https://doi.org/10.1016/j.jhazmat.2022.129378.

[32] M. Brumovský, J. Bečanová, P. Karásková, L. Nizzetto, Retention performance of three widely used SPE sorbents for the extraction of perfluoroalkyl substances from seawater, Chemosphere 193 (2018) 259–269, https://doi.org/10.1016/j.chemosphere.2017.10.174.

[33] L.A. D'Agostino, S.A. Mabury, Identification of novel fluorinated surfactants in aqueous film forming foams and commercial surfactant concentrates, Environ. Sci. Technol. 48 (2014) 121–129, https://doi.org/10.1021/es403729e.

[34] S. Barreca, M. Busetto, M. Vitelli, L. Colzani, L. Clerici, P. Dellavedova, Online solid-phase extraction LC-MS/MS: a rapid and valid method for the determination of perfluorinated compounds at sub ng·L-1 level in natural water, J. Chem. (2018) 9, https://doi.org/10.1155/2018/3780825, 2018.

[35] Y. Huang, H. Li, M. Bai, X. Huang, Efficient extraction of perfluorocarboxylic acids in complex samples with a monolithic adsorbent combining fluorophilic and anion-exchange interactions, Anal. Chim. Acta 1011 (2018) 50–58, https://doi.org/10.1016/j.aca.2018.01.032.

[36] C. Chen, J. Wang, S. Yang, Z. Yan, Q. Cai, S. Yao, Analysis of perfluorooctane sulfonate and perfluorooctanoic acid with a mixed-mode coating-based solid-phase microextraction fiber, Talanta 114 (2013) 11–16, https://doi.org/10.1016/j.talanta.2013.04.018.

[37] A.A. Olomukoro, R.V. Emmons, N.H. Godage, E. Cudjoe, E. Gionfriddo, Ion exchange solid phase microextraction coupled to liquid chromatography/laminar flow tandem mass spectrometry for the determination of perfluoroalkyl substances in water samples, J. Chromatogr. A 1651 (2021), 462335, https://doi.org/10.1016/j.chroma.2021.462335.

[38] D.T. Shoemaker, J, Method 537.1: determination of selected per-and polyfluorinated alkyl substances in drinking water by solid phase extraction and liquid chromatography/tandem mass spectrometry (LC/MS/MS), Water Qual. 1 (2018) 1–50. https://cfpub.epa.gov/si/si_public_record_Report.cfm?dirEntryId=343042&Lab=NERL. (Accessed 27 February 2020).

[39] B.K. Matuszewski, M.L. Constanzer, C.M. Chavez-Eng, Strategies for the assessment of matrix effect in quantitative bioanalytical methods based on HPLC-MS/MS, Anal. Chem. 75 (2003) 3019–3030, https://doi.org/10.1021/ac020361s.

[40] Z. Wu, W. Gao, M.A. Phelps, D. Wu, D.D. Miller, J.T. Dalton, Favorable effects of weak acids on negative-ion electrospray ionization mass spectrometry, Anal. Chem. 76 (2004) 839–847, https://doi.org/10.1021/ac0351670.

[41] Y. Hua, D. Jenke, Increasing the sensitivity of an LCMS method for screening material extracts for organic extractables via mobile phase optimization, J. Chromatogr. Sci. 50 (2012) 213–227, https://doi.org/10.1093/chromsci/bmr049.
[42] C. Monnin, P. Ramrup, C. Daigle-Young, D. Vuckovic, Improving negative liquid chromatography/electrospray ionization mass spectrometry lipidomic analysis of human plasma using acetic acid as a mobile-phase additive, Rapid Commun. Mass Spectrom. 32 (2018) 201–211, https://doi.org/10.1002/rcm.8024.
[43] F.S. Mirnaghi, J. Pawliszyn, Development of coatings for automated 96-blade solid phase microextraction-liquid chromatography-tandem mass spectrometry system, capable of extracting a wide polarity range of analytes from biological fluids, J. Chromatogr. A 1261 (2012) 91–98, https://doi.org/10.1016/j.chroma.2012.07.012.
[44] Y. Lin, R. Liu, F. Hu, R. Liu, T. Ruan, G. Jiang, Simultaneous qualitative and quantitative analysis of fluoroalkyl sulfonates in riverine water by liquid chromatography coupled with Orbitrap high resolution mass spectrometry, J. Chromatogr. A 1435 (2016) 66–74, https://doi.org/10.1016/j.chroma.2016.01.039.
[45] O.P. Togunde, E. Cudjoe, K.D. Oakes, F.S. Mirnaghi, M.R. Servos, J. Pawliszyn, Determination of selected pharmaceutical residues in wastewater using an automated open bed solid phase microextraction system, J. Chromatogr. A 1262 (2012) 34–42, https://doi.org/10.1016/j.chroma.2012.09.011.
[46] I. Bruheim, X. Liu, J. Pawliszyn, Thin-film microextraction, Anal. Chem. 75 (2003) 1002–1010, https://doi.org/10.1021/ac026162q.
[47] S. Risticevic, J. Pawliszyn, Solid-phase microextraction in targeted and nontargeted analysis: displacement and desorption effects, Anal. Chem. 85 (2013) 8987–8995, https://doi.org/10.1021/ac4003112.
[48] S. Risticevic, Solid Phase Microextraction Coupled to Comprehensive Two-Dimensional Gas Chromatography – Time-Of-Flight Mass Spectrometry for Metabolite Profiling of Apples : Potential of Non-invasive in Vivo Sampling Assay in Characterization of Metabolome, University of Waterloo, 2012. https://uwspace.uwaterloo.ca/bitstream/handle/10012/7006/Risticevic_Sanja.pdf?sequence=1&isAllowed=y.
[49] R. Jiang, J. Pawliszyn, Thin-film microextraction offers another geometry for solid-phase microextraction, TrAC, Trends Anal. Chem. 39 (2012) 245–253, https://doi.org/10.1016/j.trac.2012.07.005.
[50] S. Risticevic, H. Lord, T. Górecki, C.L. Arthur, J. Pawliszyn, Protocol for solid-phase microextraction method development, Nat. Protoc. 5 (2010) 122–139, https://doi.org/10.1038/nprot.2009.179.
[51] X. Gong, L. Xu, X. Kou, J. Zheng, Y. Kuang, S. Zhou, S. Huang, Y. Zheng, W. Ke, G. Chen, G. Ouyang, Amino-functionalized metal-organic frameworks for efficient solid-phase microextraction of perfluoroalkyl acids in environmental water, Microchem. J. 179 (2022), 107661, https://doi.org/10.1016/j.microc.2022.107661.
[52] J. Jeon, K. Kannan, B.J. Lim, K.G. An, S.D. Kim, Effects of salinity and organic matter on the partitioning of perfluoroalkyl acid (PFAs) to clay particles, J. Environ. Monit. 13 (2011) 1803–1810, https://doi.org/10.1039/c0em00791a.
[53] S. Keunchkarian, M. Reta, L. Romero, C. Castells, Effect of sample solvent on the chromatographic peak shape of analytes eluted under reversed-phase liquid chromatogaphic conditions, J. Chromatogr. A 1119 (2006) 20–28, https://doi.org/10.1016/j.chroma.2006.02.006.